COLLISION EFFICIENCY CALCULATIONS FOR SLIGHTLY DEFORMABLE AND SPHERICAL DROPS

A THESIS
SUBMITTED TO THE FACULTY
OF THE GRADUATE SCHOOL
OF THE UNIVERSITY OF MINNESOTA
BY

JOHN KARL STARK

IN PARTIAL FULFILLMENT OF THE REQUIREMENTS
FOR THE DEGREE OF
MASTER OF SCIENCE

ADVISOR: DR. MICHAEL A. ROTHER

JANUARY 2018

Acknowledgments

I would like to thank my advisor, Dr. Michael Rother, for providing helpful guidance and insight while conducting the research presented here and during the writing of this thesis, as well as for providing many beneficial opportunities during my time at the University of Minnesota Duluth. In addition, I would like to thank Dr. Keith Lodge and Dr. Steven Trogdon for serving as members of my thesis defense examination committee. Finally, I would like to thank Dr. Alexander Zinchenko, at the University of Colorado Boulder, for the use of computer code developed to accurately calculate resistance function values.

Abstract

Collision efficiency values are calculated for both slightly deformable drops and spherical drops (as applied to raindrop growth). The calculation of these values is important in performing population dynamics modeling to determine drop size distributions occurring in various applications, such as in raindrop formation. The results presented here for slightly deformable drops, for small Reynolds numbers and Marangoni numbers, subjected to combined gravitational and thermocapillary driving forces, show variations in collision efficiency values with changing values of the parameter N_V, the ratio of the isolated gravitational drop velocity to that of the isolated thermocapillary drop velocity, $\hat{\mu}$, the drop-to-medium viscosity ratio, and $\hat{k}$, the drop-to-medium thermal conductivity ratio. Namely, increases in $\hat{\mu}$ and $\hat{k}$ lead to significant decreases in the collision efficiency values calculated at the same value of N_V and the same value of k, the drop size ratio. While for spherical drops, as applied to raindrop growth, it is shown, for small Reynolds numbers, that the inclusion of combinations of accurately calculated Maxwell slip and retarded or unretarded van der Waals forces increases the collision efficiency values calculated for certain drop sizes and drop size ratios. Lubrication forces, hydrodynamic forces, internal drop circulation, weight, and buoyancy are also included in the calculations, so that the resulting collision efficiencies are that much more indicative of the natural process of raindrop growth.

Contents

List of Figures

Nomenclature

a_1	Radius of smaller drop
a_2	Radius of larger drop
A	Hamaker constant
b	A parameter having the same order of magnitude as the dimple radius
Ca	Capillary number
d_∞^*	Critical offset between two interacting drops
E_0	Collision efficiency for spherical drops without interparticle forces
E_{12}	Collision efficiency
F	Force
g	Gravitational acceleration
$\hat{g}$	Gravity vector
G	Mobility function for an equal-and-opposite force parallel to the line-of centers of the drops (Rother, Zinchenko, and Davis, 1997, [33])
h	Film thickness between two interacting drops
k	Drop size ratio
k_d	Drop thermal conductivity
k_e	External fluid medium thermal conductivity
$\hat{k}$	Drop-to-medium thermal conductivity ratio
L	Mobility function for gravitational motion parallel to the line-of-centers of the drops
L_M	Mobility function for thermocapillary motion parallel to the line-of-centers of the drops

m_2	Mass of the larger drop
M	Mobility function for gravitational motion perpendicular to the line-of-centers of the drops
M_M	Mobility function for thermocapillary motion perpendicular to the line-of-centers of the drops
Ma	Marangoni number
N_F	Term allowing for combination of gravitational and thermocapillary driving forces
N_V	Ratio of gravitational-to-thermocapillary relative drop velocities
p	Pressure
Q_{12}	Interparticle force
r	Position vector
$\hat{r}$	Position vector
R	Reduced radius
Re	Reynolds number
s	Dimensionless drop separation
St	Stokes number
t	Time
T_{ij}	Resistance functions
$\nabla T, \nabla T_\infty$	Temperature gradient
u	Velocity
V_1	Velocity of drop 1
V_2	Velocity of drop 2
$V_{G,12}^{(0)}$	Gravitational relative drop velocity

$V_{M,12}^{(0)}$	Thermocapillary relative drop velocity
α_G	Gravitational driving force
α_M	Thermocapillary driving force
$\beta(t)$	Angular component of combined gravitational-thermocapillary driving force
β_0	Initial angle between two interacting drops
β_c	Critical angle calculated for two interacting drops
δ	Non-dimensional Hamaker parameter
ζ	A term included in $\beta(t)$ that accounts for M and M_M
θ	New angle between two interacting drops
θ_0	Initial angle between two interacting drops
λ_L	Mean free path of air
Λ_{ij}	Resistance functions
$\hat{\mu}$	Drop-to-medium viscosity ratio
μ_d	Drop viscosity
μ_e	External fluid medium viscosity
ξ	Gap distance between two interacting drops
ρ_d, ρ'	Density of fluid composing drops
ρ_e, ρ	Density of external fluid medium surrounding drops
γ, σ	Interfacial tension
$\Phi_{12,ret}$	Dimensionless interparticle potential for retarded van der Waals forces
$\Phi_{12,unret}$	Dimensionless interparticle potential for unretarded van der Waals forces

Chapter 1

Introduction

The calculation of collision efficiency values for the interactions of drops has been studied in much detail over the last fifty to sixty years. As these values play critical roles in determining, for example, size distributions used for modeling raindrop growth in atmospheric models, it is important that the accuracy of such calculations is as great as possible, to ensure that the models, as nearly as possible, predict physical reality. The goals of the following chapters are threefold: to present some historical context of the work done to the present on both slightly deformable drops and spherical drops, to present modified theoretical frameworks to calculate collision efficiency values, and finally, to present the results obtained through the newly developed theory. Chapter 2 focuses on slightly deformable drops, while Chapter 3 shifts to spherical drops and applications to raindrop growth. Both chapters discuss the calculation of collision efficiencies for their respective scenarios.

Chapter 2

Collision Efficiency Calculations:

Slightly Deformable Drops

Studies of drop interactions and coalescence are numerous. Up to the present, several theoretical studies have been conducted in an effort to calculate collision efficiencies for droplet-droplet interactions due to a gravitational driving force, a thermocapillary driving force, a combined gravitational and thermocapillary driving force, and others as well, such as Brownian motion. Work by Zhang, Wang, and Davis (1993, [49]) studied the scenario of a combined gravitational-thermocapillary driving force for spherical drops, introducing a parameter N_V, the ratio of the gravitational relative drop velocity to the thermocapillary relative drop velocity, thereby representing the dominating driving force for the system interaction. They were able to show that when the driving forces were oppositely aligned, a collision-forbidden region existed in which coalescence would not occur after the drops had reached a critical size. Rother, Zinchenko, and Davis (1997, [33]) and later, Rother and Davis (1999, [30]), presented collision efficiency calculations for slightly deformable drops interacting due to solely gravitational and solely thermocapillary driving forces, respectively. Rother and Davis (2005, [32]) also studied the interactions of drops and bubbles due to a combination of thermocapillary and gravitational driving forces, while allowing for large deformations in the surfaces of the drops and bubbles. Finally, Rother and Davis (2001, [31])

investigated the interactions of slightly deformable drops in different flows, while including unretarded van der Waals forces. Thus, it is only natural that this work should be extended to deal with the combined gravitational and thermocapillary driving forces acting on slightly deformable drops, and thus, is the subject of this chapter.

Several other papers have focused on different aspects relating to droplet interactions. Janssen and Anderson (2011, [15]) examined, broadly, the work completed in many areas of study related to drop interactions. As experimental results can be difficult to obtain, a number of papers deal mainly with theoretical computations. Bazhlekov, Chesters, and van de Vosse (2000a, [2]) were able to develop an explicit numerical scheme to study the dynamics of the thin film between two drops in close approach for different drop-to-medium viscosity ratios. Their results were found to be comparable to those of Rother, Zinchenko, and Davis (1997, [33]). Bazhlekov, van de Vosse, and Chesters (2000b, [3]) also investigated rim and nose rupture for two interacting drops. Other numerical work, focusing on boundary-integral algorithms, has been completed by Zinchenko, Rother, and Davis (1997, [52]) and Rother, Zinchenko, and Davis (2002, [34]).

Also included in theoretical computational work is population dynamics modeling. Ismail and Loewenberg (2004, [14]) performed population dynamics modeling to study the drop size distributions generated for different flows and driving forces but did not include drop deformation. Work by Wang and Davis (1993, [39]) studied the coalescence of drops through population dynamics modeling, resulting from Brownian motion, gravity, and thermocapillary driving forces, separately. Nas and

Tryggvason (2003, [22]) studied, numerically, the interactions of deformable drops and bubbles due to a thermocapillary driving force.

While the present paper deals with surfactant-free drops, Rother (2009, [28]) has studied the effects of surfactants on the interactions of spherical drops moving due to a thermocapillary driving force. Rother (2007, [27]) has also studied how surfactants affect the coalescence of deformable drops moving due to a thermocapillary driving force and a combined gravitational-thermocapillary driving force (Rother, 2013, [29]).

Experimental work has been performed, none the less, by several authors. Fortelný and Jůza (2014, [9]) studied drop coalescence in a flow for both monodispersed and polydispersed systems and found that coalescence decreases for polydispersed drop systems. Fortelný and Jůza (2015, [10]) also studied experimentally how the fluid medium surrounding two drops can impact the collision efficiency calculations. Experimental work was conducted by Kang et al. (2006, [17]) to study thermocapillary and buoyancy effects on interactions of different-sized drops. Young, Goldstein, and Block (1959, [45]) studied how temperature can affect the movement of bubbles. Zhang, Duan, and Kang (2016, [48]) used a holographic method to experimentally study the motion of drops due to a thermocapillary driving force. Finally, experimental work by Dai et al. (2016, [6]) studied paraffin oil drops moving due to a thermocapillary driving force.

Theoretical work related to the topic of collision efficiency calculations can be grouped into two major categories: work concerned with gravitational motion and work concerned with thermocapillary motion. Gravitational motion studies are numerous.

Yiantsios and Davis (1991, [44]) investigated the interactions of drops subjected to a gravitational driving force, as well as accounting for the effects of van der Waals forces. Zhang and Davis (1991, [46]) studied the impacts of gravitational and Brownian motion driving forces on the coalescence of spherical drops, while Wang and Davis (1996, [40]) studied the effects of combining these two driving forces. Baldessari, Homsy, and Leal (2007, [1]) studied the film drainage between two equal-sized drops for small capillary numbers. Finally, Ramirez, Zinchenko, Loewenberg, and Davis (1999, [25]) looked at the effects of Brownian motion and convection on the flotation of spherical particles, while also accounting for van der Waals forces.

The other major category, that of thermocapillary motion, also includes numerous studies. Berejnov, Lavrenteva, and Nir (2001, [4]) studied thermocapillary interactions of deformable drops of equal and different sizes. Zhang and Davis (1992, [47]) studied the calculation of collision efficiencies for spherical drops moving due to a thermocapillary driving force. Keh and Chen (1992, [18]) studied the thermocapillary motion of spherical drops and bubbles in lines of different lengths having various properties. Zhou and Davis (1996, [50]) investigated, for deformable drops, thermocapillary motion and the effects of changing the values of the drop size ratio, the capillary number, and the thermal conductivity ratio. Berejnov, Leshanksy, Lavrenteva, and Nir (2002, [5]) studied thermocapillary motion of both spherical and deformable drops using asymptotic and boundary-integral methods. Mahesri, Haj-Hariri, and Borhan (2014, [21]) investigated deformable drops moving due to a thermocapillary driving force inside of an insulated cylinder. Xie et al. (2016, [43]) studied deformable drops moving

due to a thermocapillary driving force. Both the finite difference method and lattice Boltzmann method were used. Finally, Wozniak (1991, [42]) studied thermocapillary drop interactions for situations where gravitational forces are negligible.

An important motivating study for the work presented here was presented by Zinchenko and Davis (2005, [51]) on the development of a multipole-accelerated algorithm for performing calculations for the interactions of slightly deformable drops. Two of the major assumptions employed in the calculations and present theory are that of local axisymmetry in the gap region between two drops in close approach and neglecting the pumping flow effect. The pumping flow effect is simply the effect experienced when two slightly deformable drops are in apparent contact. As the drops move relative to one another, the driving force pushing the drops together displaces liquid from the gap region between the drops. This results in liquid being squeezed out from between the drops and, therefore, a pressure reduction. This in turn has the opposite effect of then causing liquid to enter the gap region to balance the displacement. This pumping effect inhibits coalescence and decreases collision efficiencies. The assumption for this work is that since the drops are in apparent contact for a very limited amount of time, the pumping flow effect will not significantly impact collision efficiency calculations. Previous work regarding the gap region between two spherical drops was conducted by Davis, Schonberg, and Rallison (1989, [8]). Zinchenko and Davis (2005, [51]) were able to verify that these assumptions are valid for the system considered in this study, and that, in particular, previous work, utilizing leading-order asymptotic calculations, was valid for $Ca \ll 1$ and $\hat{\mu} = O(1)$.

2.1 Problem Statement and Formulation

The problem of calculating collision efficiencies for two interacting drops has been solved, presently, for the case of combined gravitational and thermocapillary driving forces, as well as for the inclusion of van der Waals forces and slight drop deformation. Therefore, the present problem is complicated by several factors not previously considered in similar studies. The Appendix includes a brief discussion of the dimensionless thin-film equations, presented in previous studies (Rother, Zinchenko, and Davis, 1997, [33]; Rother and Davis, 1999, [30]; Zinchenko and Davis, 2005, [51]), governing the inner region of close-approach of the two interacting drops and will not be discussed further here. Figure 2.1 shows the interaction of two slightly deformable drops moving due to a combined gravitational-thermocapillary driving force. It should be noted that the temperature gradient can be aligned parallel in the same direction, or parallel in the opposite direction, of the applied gravitational field.

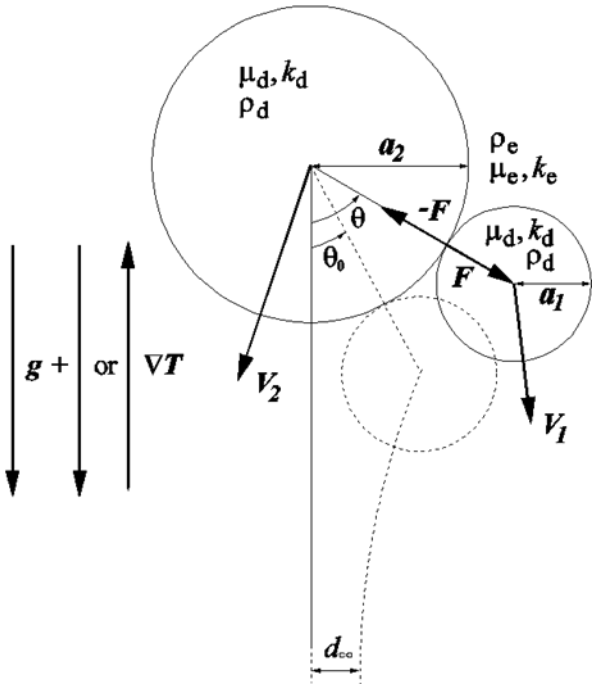

Figure 2.1 Interaction of two slightly deformable drops subjected to a combined gravitational-thermocapillary driving force. Note that the temperature gradient can be aligned in the same or opposite direction of the downward-pointing gravity field (Stark and Rother, 2016, [36]).

At the low Reynolds numbers considered, the Stokes equations are linear and allow for some simplifications to be made when solving for the forces acting on the drops. By including the deformation of the drops, hydrodynamic forces between the drops, interparticle forces, and the combined thermocapillary and gravitational motion of the drops, collision efficiency values can be calculated. In order to calculate the collision efficiency values, it is necessary to determine β_c, or the critical angle between the two drops that will lead to a horizontal offset just resulting in coalescence. When β_c is known for a certain set of parameters, the collision efficiency can be calculated from the following (Rother, Zinchenko, and Davis, 1997, [33]):

$$E_{12} = (\sin^2 \beta_c) E_0. \tag{2.1}$$

E_0 in (2.1) represents the collision efficiency calculated for spherical drops in the absence of interparticle forces and is calculated through the evaluation of the following integral (Zhang, Wang, and Davis, 1993, [49]):

$$E_0 = \exp\left(2\int_2^{\infty} \frac{(L-M) + \left(\frac{1}{N_V}\right)(L_M - M_M)}{s\left[\left(\frac{1}{N_V}\right)L_M + L\right]} ds \right). \tag{2.2}$$

The modifications that were made to account for the combined driving forces and the angular dependence of the problem are presented henceforth.

First, it is necessary to define the parameters used in this study. The key parameters include the following: the size ratio of the smaller drop to that of the larger drop $k = \frac{a_1}{a_2}$, the drop-to-medium viscosity ratio $\hat{\mu} = \frac{\mu_d}{\mu_e}$, the drop-to-medium thermal conductivity ratio $\hat{k} = \frac{k_d}{k_e}$, and the ratio of the relative drop velocities due to gravitational and thermocapillary driving forces, respectively, $N_V = \pm\frac{V_{G,12}^0}{V_{M,12}^0}$. Here, the $\pm$ symbol indicates that the gravitational and thermocapillary driving forces can be aligned in the same direction $(+)$ or aligned in opposing directions $(-)$. N_V can also be defined in terms of various parameters as follows (Zhang, Wang, and Davis, 1993, [49]):

$$N_V = \pm\frac{(\hat{\mu}+1)\left(\hat{k}+2\right)|\rho' - \rho|(a_1 + a_2)g}{3\left|\left(\frac{\partial\gamma}{\partial T}\right)\nabla T_{\infty}\right|}. \tag{2.3}$$

In (2.3), $\hat{\mu}$ is the drop-to-medium viscosity ratio, $\hat{k}$ is the drop-to-medium thermal conductivity ratio, ρ' is the drop fluid density, ρ is the surrounding medium density, a_1 and a_2 are the drop radii, g is the gravity vector, $\frac{\partial\gamma}{\partial T}$ is the interfacial tension change with

temperature, and ∇T_∞ is the temperature gradient present far from the drops. Finally, the Hamaker parameter, δ, is also of importance, where

$$\delta = \frac{\pi^2}{3}\frac{A\sigma^2}{(\Delta\rho g)^3}\frac{1}{R^8}\,. \tag{2.4}$$

As stated previously, it was necessary to modify the governing thin-film equations for the inner region (see the Appendix for a further discussion) in order to account for the combined gravitational-thermocapillary driving force. To do this, the equations were made non-dimensional using the following term that includes the parameter b, which is of the same order of magnitude as that of the dimple radius, and σ, which is the interfacial tension:

$$\frac{\pi b^2\sigma}{R} = \Delta\rho g R^3. \tag{2.5}$$

Here, R, the reduced radius, is defined as follows:

$$R = \frac{a_1 a_2}{a_1 + a_2}. \tag{2.6}$$

The main differences appear in the integral force balance, which is shown below in (2.7):

$$\int_0^\infty \left(p - \frac{\delta}{h^3}\right) r dr = [\alpha_G \pm N_F \alpha_M]\cos\beta(t)\,. \tag{2.7}$$

N_F is defined as

$$N_F = \pm\frac{(\hat{\mu}+1)\left(\hat{k}+2\right)(1+k)^2}{3kN_V}. \tag{2.8}$$

The N_F term is necessary in order to combine the two driving forces, namely the gravitational and thermocapillary driving forces, α_G and α_M, respectively. The gravitational and thermocapillary driving forces are defined as follows:

$$\alpha_G = \frac{4\pi(1-k^2)(1+k)^2}{3k^2}\lim_{\xi\to 0}\frac{L}{G} \tag{2.9}$$

and

$$\alpha_M = \frac{4\pi(1-k^2)}{(\hat{\mu}+1)(\hat{k}+2)k}\lim_{\xi\to 0}\frac{L_M}{G}, \tag{2.10}$$

respectively. These two terms, α_G and α_M, include the mobility functions for motion parallel to the line-of-centers of the two interacting drops. $\beta(t)$ accounts for the time-dependence of the angular component of the driving force and is defined as follows:

$$\beta(t) = 2\arctan\left[\tan\left(\frac{\beta_0}{2}\right)\exp\left(\zeta Ca^{\frac{1}{2}}t\right)\right]. \tag{2.11}$$

Finally, ζ includes the mobility functions for motion perpendicular to the line-of-centers of the two interacting drops and is defined as follows:

$$\zeta = \frac{2\hat{\mu}}{3(1+k)}\sqrt{\frac{2\pi(1-k^2)(\hat{\mu}+1)}{\hat{\mu}+\frac{2}{3}}}\lim_{\xi\to 0}\left(M \pm \frac{1}{N_V}M_M\right). \tag{2.12}$$

The computer code used to calculate the critical angles was modified to account for these changes to the integral force balance. This computer code is available upon request.

2.2 Results and Discussion

In order to study the effects of various parameter values on the collision efficiencies calculated, a parameter-space investigation was conducted. The parameters modified included $\hat{\mu}$, $\hat{k}$, and N_V. Figure 2.2 and Figure 2.3 show collision efficiencies calculated for both spherical drops and slightly deformable drops for negative and positive values of N_V, respectively. The following combinations of $\hat{\mu}$ and $\hat{k}$ were used:

$\hat{\mu} = \hat{k} = 1$, $\hat{\mu} = \hat{k} = 2$, and $\hat{\mu} = \hat{k} = 5$. The range of N_V values used was -20 to 20. Finally, the spherical drop results, from work completed by Zhang, Wang, and Davis (1993, [49]), are shown as dashed lines, while the slight-deformation results are shown as solid lines.

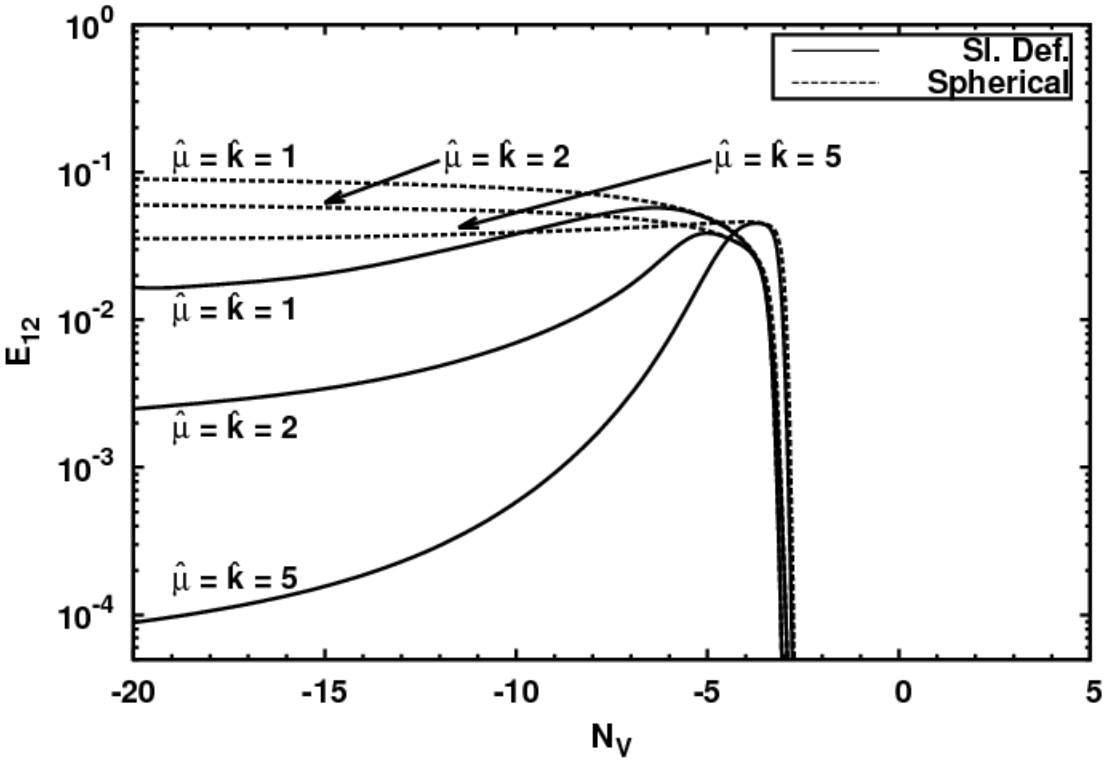

Figure 2.2 Collision efficiencies for spherical drops (Zhang, Wang, and Davis, 1993, [49]) and slightly deformable drops for $k = 0.5$ and $\delta = 0.0001$ and for different values of N_V, $\hat{\mu}$, and $\hat{k}$.

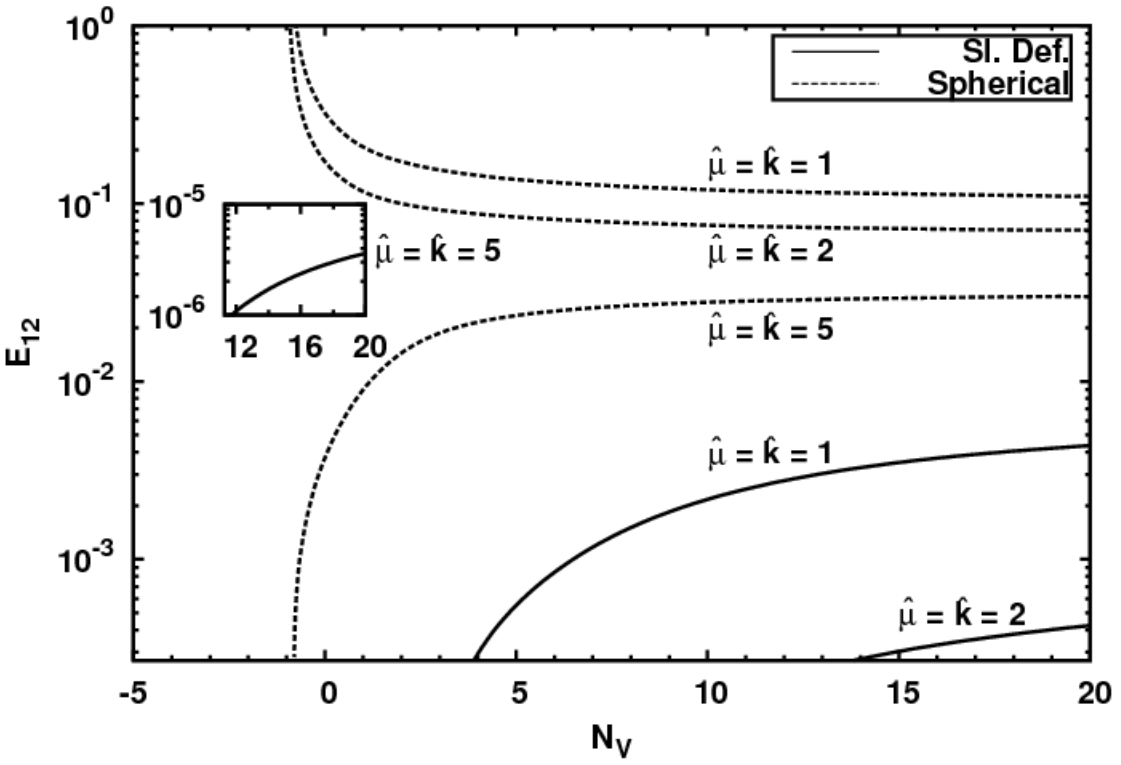

Figure 2.3 Collision efficiencies for spherical drops (Zhang, Wang, and Davis, 1993, [49]) and slightly deformable drops for $k = 0.5$ and $\delta = 0.0001$ and for different values of N_V, $\hat{\mu}$, and $\hat{k}$.

As stated previously, the ratio, N_V, represents the relative contributions of gravitational-to-thermocapillary driving forces, respectively. Also, negative values of N_V indicate that these two driving forces are opposed, or directed in opposite directions, while positive values of N_V indicate that the two driving forces are aligned in the same direction.

The general trends observed in Figure 2.2 and Figure 2.3 are that as the drop-to-medium viscosity ratio and the drop-to-medium thermal conductivity ratio increase in magnitude, the effect of drop deformation becomes much more pronounced and apparent, as deviations from the spherical drop results, and the collision efficiency values decrease significantly.

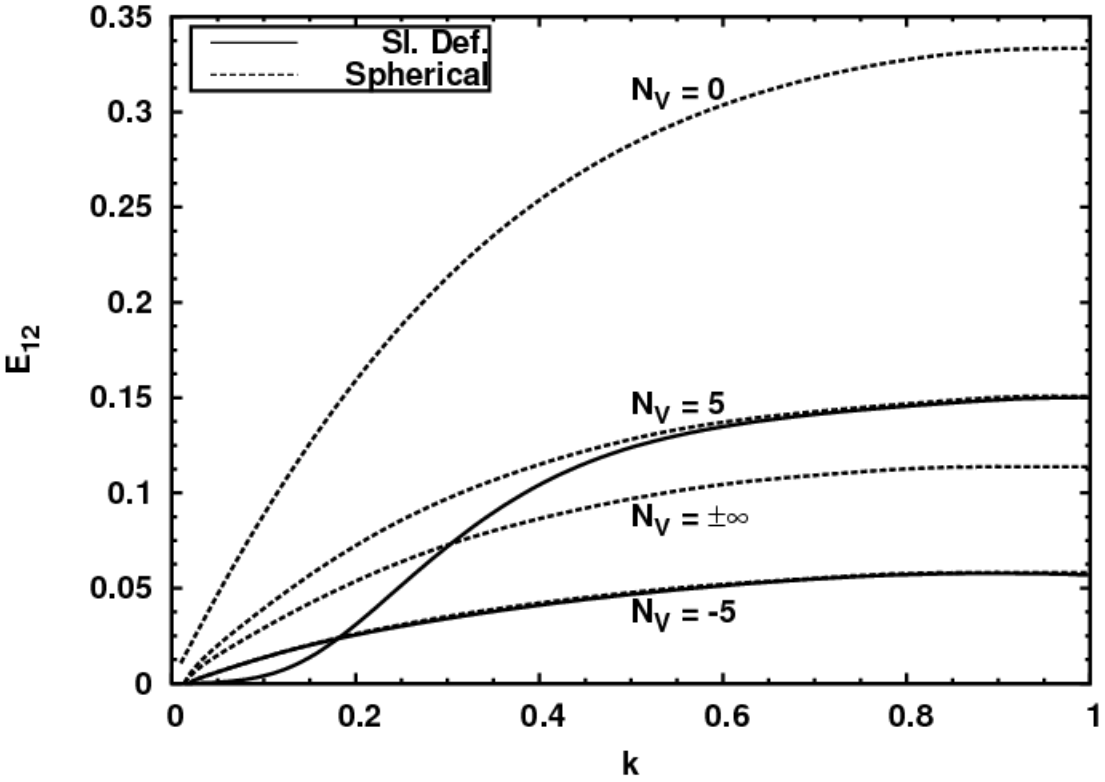

Figure 2.4 Collision efficiencies for spherical drops (Zhang, Wang, and Davis, 1993, [49]) and slightly deformable drops for different values of N_V and k and $\hat{\mu} = \hat{k} = 1$. $\delta = 0.01$ for $N_V = 5$ and $\delta = 1$ for $N_V = -5$.

Finally, Figure 2.4 presents collision efficiency values calculated for different drop size ratios, k, at constant values of N_V. The curves for $N_V = 0$ and $N_V = \pm\infty$ are presented as references. Collision efficiencies were calculated for slightly deformable drops for both $N_V = -5$ and $N_V = 5$. When N_V is positive, and the driving forces are aligned in the same direction, the effects of drop deformation are observable. When the value of the Hamaker parameter, δ, is $O(1)$, deviation from the spherical drop results is essentially non-existent for $N_V = -5$. Additional curves, at other values of N_V, may help to support these observations.

Chapter 3

Collision Efficiency Calculations:

Spherical Drops (Raindrop Growth)

Chapter 2 presented theory and collision efficiency calculations for drops when allowing for small deformations to occur on the surfaces of the drops. The allowance for slight deformation of the drops increases the complexity of the problem. The aim of Chapter 3 is to move from a purely theoretical discussion to one of more theory and application. Atmospheric modeling is a very important tool that allows for the prediction of atmospheric phenomena, such as that of raindrop growth. The goal of the present work is to calculate collision efficiency values for water drops in air and compare the results with those of three different journal articles, namely: Klett and Davis (1973, [19]), Pinsky et al. (2001, [24]), and Wang et al. (2005, [41]).

Much work has been done in the past to study raindrop growth and the development of raindrop size distributions in the atmosphere. Past work has assumed that the drops are solid spheres. Hocking (1959, [12]) investigated the calculation of collision efficiency values for water drops in air having maximum radii of 30 μm and determined that drops having radii less than or equal to 18 μm would not collide. Davis and Sartor (1967, [7]) calculated collision efficiency values and showed that drops having radii less than 19 μm will, in fact, interact and collide. Hocking and Jonas (1970, [13]) investigated the significance of the gap size cutoff, ϵ, used to determine if two drops

have, in fact, collided. They found that using an incorrect value for ϵ could result in lower-than-actual collision efficiencies. No attractive forces, such as van der Waals forces, were included in the calculations. This paper also noted the importance of finding a way to account for the fact that the gap between two drops may be smaller than the mean free path of air molecules. This is something that is accurately accounted for in the present results, where the mean free path of air molecules is assumed to be $\lambda_L \approx 0.1\ \mu m$. Jonas (1972, [16]) calculated collision efficiencies for water drops in air, and by modifying earlier results that accounted for the boundary conditions when the gap between the drops was on the order of, or smaller than, the mean free path of air molecules, he found that using a gap value of approximately 1.3 times the mean free path of air increased the collision efficiencies calculated versus those calculated by Hocking and Jonas (1970, [13]).

Klett and Davis (1973, [19]) extended much of the previous work completed to that point to drops of larger sizes, namely, up to drop radii of 70 μm. They used a modified superposition method to calculate the forces on the drops. Lin and Lee (1975, [20]) studied linear collision efficiency calculations for water drops in air using the superposition method. It was found that the size of the drops relative to one another can greatly affect the collision efficiency value for an interaction. Schlamp, Grover, Pruppacher, and Hamielec (1976, [35]) found that collision efficiency values calculated for electrically charged water drops in air, subjected to an electric field, will be greater than when no electric charge or electric field is present. Hall (1980, [11]) found that the inclusion of ice in models will have an effect on the collision efficiency values

calculated, as well. Rogers and Davis (1990, [26]) performed population dynamics modeling and investigated the effects of including combinations of slip boundary conditions and van der Waals forces on the collision efficiency values calculated and found that values increased. It should be noted that the calculation of the slip conditions was not exact, as is the case in the present work.

Pinsky, Khain, and Shapiro (2001, [24]) expanded the range of collision efficiency calculations by including drops with maximum radii of 300 μm and maximum Reynolds number values of 100. They also found that the height in the atmosphere at which drop interactions occur will greatly impact collision efficiency values. Wang et al. (2005, [41]) modified the superposition method that was extensively used in early models for water drop growth in air. They were able to reduce the errors found in earlier calculations by better accounting for boundary conditions. Vohl et al. (2007, [38]) performed experiments for drops having radii up to 170 μm and were able to generate large tables of collision efficiency values for different drop size ratios. Finally, Pinsky, Khain, and Krugliak (2008, [23]) investigated the effects of turbulence on the collision efficiency values calculated for water drops in air.

The significance of the calculations and results presented henceforth are that the collision efficiencies are calculated for spherical, liquid drops while accounting for the following: combinations of Maxwell slip and van der Waals forces (calculations are included for both retarded and unretarded van der Waals forces), rather than each case individually. The necessary allowances are also made to account for the weight of the drops, buoyant forces, hydrodynamic interactions between the drops, lubrication forces

when the drops are in close approach, and internal drop circulation. The computer code used to calculate the critical offset between the drops was modified accordingly to study the different combinations of Maxwell slip and van der Waals forces.

3.1 Problem Description and Formulation

As was done in Chapter 2, two unequal-size drops moving in relative motion to one another are considered. Here it is further assumed that the drops are composed of water dispersed in air. Figure 3.1 shows the two drops falling under a downward-pointing gravitational field.

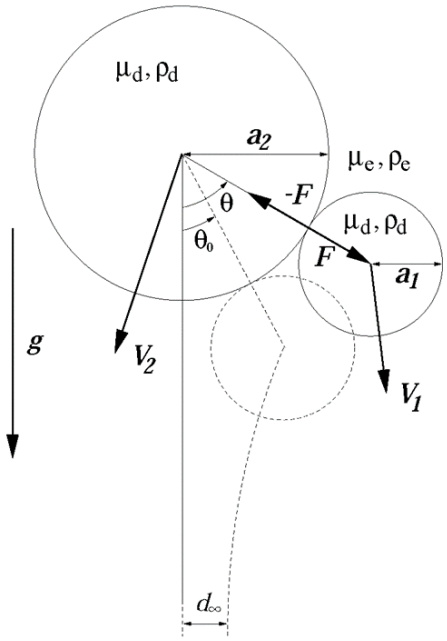

Figure 3.1 Interaction of two spherical liquid drops subjected to a gravitational driving force (Stark and Rother, 2017, [37]).

Important dimensionless parameters considered in this chapter are the following: the drop size ratio $k = \frac{a_1}{a_2}$, the drop-to-medium viscosity ratio $\hat{\mu} = \frac{\mu_d}{\mu_e}$, and the collision efficiency

$E_{12} = \left(\frac{d_\infty^*}{a_1+a_2}\right)^2$, which depends on the drop radii and the critical offset, d_∞^*, calculated in order for the drops to just make contact. In subsequent calculations, d_∞^* is scaled by the radius of the larger drop, a_2. The drops are now considered spheres, whereas the drops in Chapter 2 were allowed to deform slightly. It is also important to note that the Reynolds number was assumed to be small but non-zero ($0.01 < Re < 0.3$). Over the range of drop radii considered (maximum radius of 30 μm), the Stokes number is always larger than the Reynolds number ($1 < St < 100$). This makes the water – air system different because a low Reynolds number does not necessarily mean that the drop inertia is negligible, as was considered in Chapter 2. Due to the possibility of significant drop inertia, the force balance that must be solved does not equal zero, and, therefore, the resulting velocity equations are nonlinear. The equations that result and must be solved are shown below in (3.1) and (3.2) (Stark and Rother, 2017, [37]). Expressions for the calculation of both retarded and unretarded van der Waals forces are also given below in (3.4) and (3.5), respectively (Stark and Rother, 2017, [37]).

$$k^2 St \frac{dV_1}{dt} = k^2 \left(\frac{\hat{\mu} + \frac{2}{3}}{\hat{\mu} + 1}\right) \hat{g} - \left[\Lambda_{11}(V_1 - V_2)^{\parallel} + \Lambda_{12} V_2^{\parallel} + T_{11}(V_1 - V_2)^{\perp} + T_{12} V_2^{\perp}\right] \quad (3.1)$$

$$St \frac{dV_2}{dt} = k^2 \left(\frac{\hat{\mu} + \frac{2}{3}}{\hat{\mu} + 1}\right) \hat{g} - \left[\Lambda_{21}(V_1 - V_2)^{\parallel} + \Lambda_{22} V_2^{\parallel} + T_{21}(V_1 - V_2)^{\perp} + T_{22} V_2^{\perp}\right] \quad (3.2)$$

In (3.1) and (3.2), St represents the Stokes number and is defined as follows (Stark and Rother, 2017, [37]):

$$St = \frac{m_2 \frac{V_2^0}{t_s}}{6\pi\mu_e a_2 V_2^0} = \frac{4}{81}\left(\frac{\hat{\mu}+1}{\hat{\mu}+\frac{2}{3}}\right)\left(\frac{\rho_d|\rho_d-\rho_e|g}{\mu_e^2}\right)a_2^3. \tag{3.3}$$

Also, in (3.1) and (3.2), Λ_{ij} and T_{ij} are resistance functions.

$$F_{mol,i} = \pm\frac{k(1-k^2)}{2}\left(\frac{\hat{\mu}+\frac{2}{3}}{\hat{\mu}+1}\right)\frac{1}{Q_{12}}\frac{d\Phi_{12,ret}}{dr}\hat{r} \tag{3.4}$$

$$F_{mol,i} = \pm\frac{k(1-k^2)}{2}\left(\frac{\hat{\mu}+\frac{2}{3}}{\hat{\mu}+1}\right)\frac{1}{Q_{12}}\frac{d\Phi_{12,unret}}{dr}\hat{r} \tag{3.5}$$

In (3.4) and (3.5), Q_{12} is defined as follows (Stark and Rother, 2017, [37]):

$$Q_{12} = \frac{2\pi}{3}k(1-k^2)\frac{|\rho_d-\rho_e|ga_2^4}{A}. \tag{3.6}$$

Also, in (3.4) and (3.5), $\frac{d\Phi_{12,ret}}{dr}$ and $\frac{d\Phi_{12,unret}}{dr}$ are the dimensionless interparticle potentials for retarded and unretarded van der Waals forces, respectively. In (3.6), A is the Hamaker constant.

3.2 Results and Discussion

The first results presented in Figure 3.2 show how collision efficiencies change for varying larger drop radii, a_2, at a constant drop size ratio of $k = 0.5$. Drop radii cover the range of 2 μm to 50 μm. The smallest collision efficiency values were calculated when no van der Waals forces were included. On the other hand, a combination of Maxwell slip and unretarded van der Waals forces produced the largest collision

efficiency values, as would be expected. The most realistic curve to note is that for the combination of Maxwell slip and retarded van der Waals forces, which falls just below the curve for Maxwell slip and unretarded van der Waals forces.

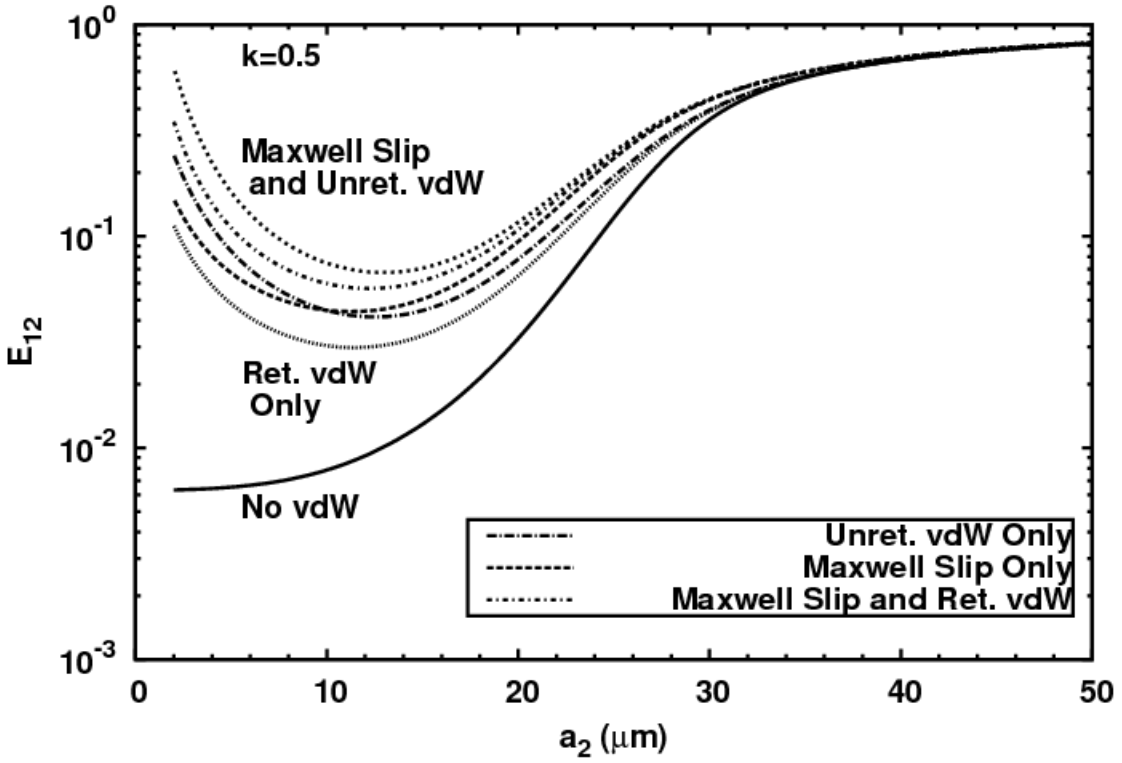

Figure 3.2 Collision efficiencies calculated for spherical liquid drops for different larger drop radii and a constant drop size ratio of $k = 0.5$. The collision efficiency data point for $a_2 = 2\ \mu m$ was calculated by M. A. Rother (Stark and Rother, 2017, [37]).

Now that it was shown how collision efficiencies vary with the larger drop radius, results for different size ratios for specific larger drop radii are presented in Figure 3.3.

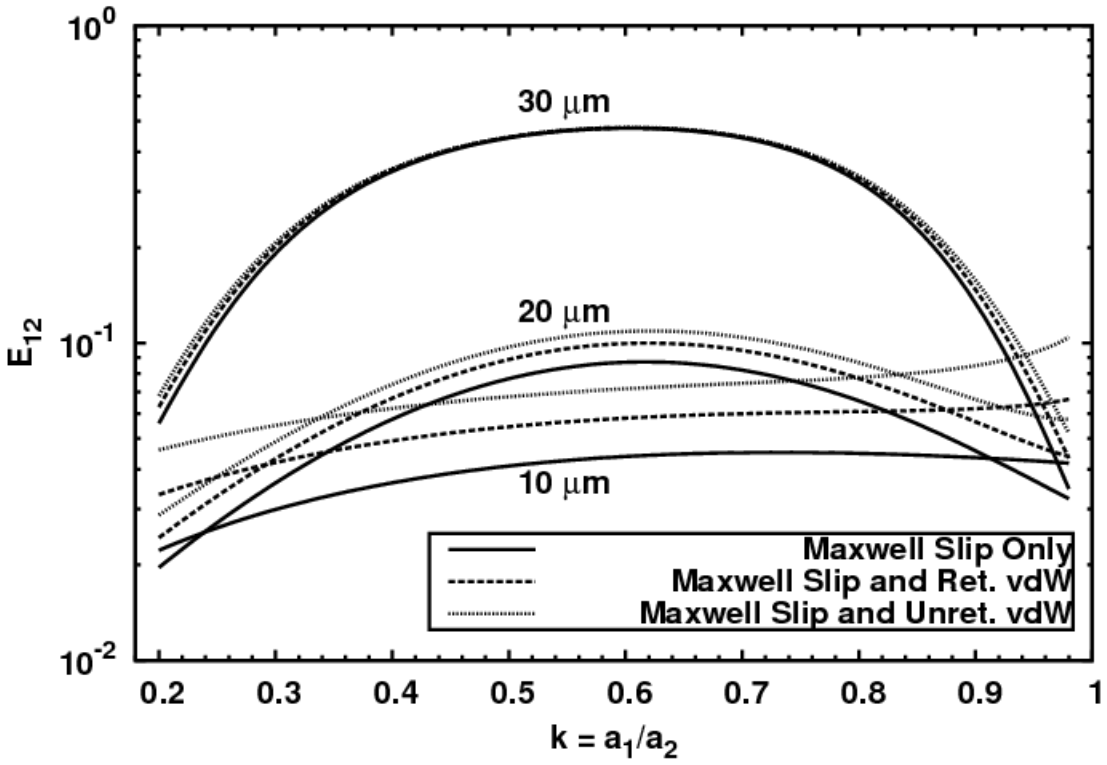

Figure 3.3 Collision efficiencies calculated for spherical liquid drops over a range of drop size ratios, k, for different values of the larger drop radius, a_2.

The important feature to note in Figure 3.3 is that the effects of van der Waals forces on calculated collision efficiency values are dependent on the drop sizes. For smaller drops, the interparticle forces are important, and it can be seen that collision efficiency values increase with the inclusion of van der Waals forces. At drop sizes of 30 μm and larger, inertial effects begin to dominate, whereas the effects of Maxwell slip and combinations of retarded and unretarded van der Waals forces diminish. The final three figures serve as comparisons between the current calculations and previous studies investigating raindrop growth.

Figure 3.4 shows data from a study performed by Klett and Davis in 1973 [19], for small Reynolds number values. The method of solution employed by Klett and Davis

was that of superposition. The use of this method does not properly account for lubrication forces in the gap region between two drops when they are nearly touching. This tends to result in higher-than-predicted collision efficiency values for some drop sizes. Their data was in fairly close agreement over the range of size ratios of $k = 0.5$ to $k = 0.98$ when the current calculations included a combination of Maxwell slip and retarded van der Waals forces. At smaller values of k, Klett and Davis underpredicted the collision efficiency values.

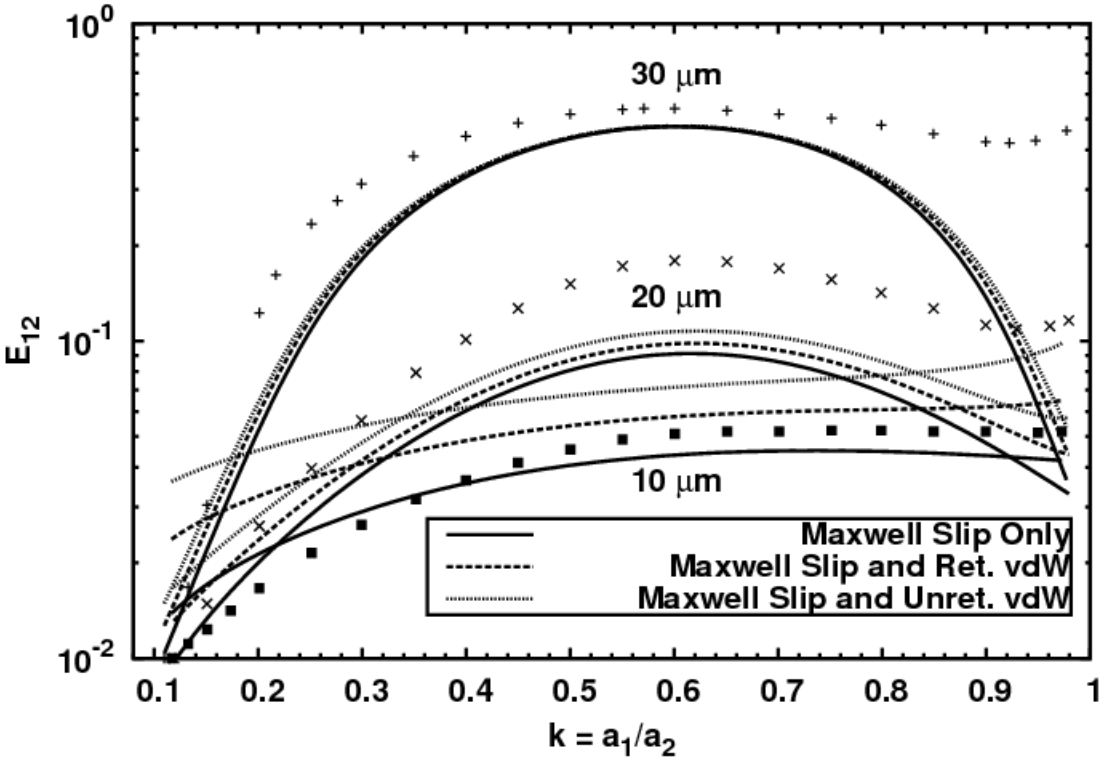

Figure 3.4 Comparison with data produced by Klett and Davis (1973, [19]) for water drops in air. ■, x, and + represent their data for larger drop radii of 10 μm, 20 μm, and 30 μm, respectively.

The next comparison made was to data generated by a study conducted by Pinsky et al. in 2001 [24]. Again, a superposition method was used to solve the force balance on the drops, and, therefore, does not properly account for lubrication forces between the

drops. Figure 3.5 shows the results from their 2001 study and the present results for larger drop radii of 20 μm and 30 μm for different drop size ratios, k. As with the data produced by Klett and Davis (1973, [19]), the data generated by Pinsky et al. (2001, [24]) shows an overestimation of the collision efficiency values for the larger drop radius of 30 μm. At the smaller drop size ratios, their data shows larger underestimations of the collision efficiency values at both larger drop radii of 20 μm and 30 μm.

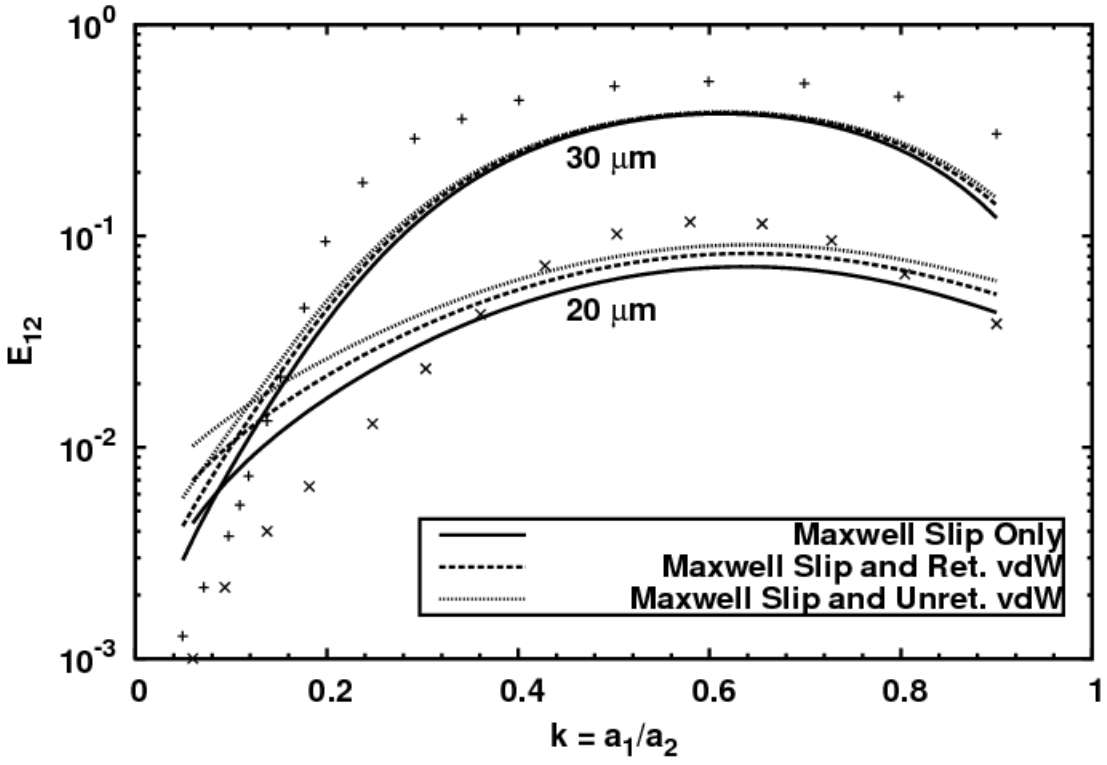

Figure 3.5 Comparison with data produced by Pinsky et al. (2001, [24]) for water drops in air. x and + represent their data for larger drop radii of 20 μm and 30 μm, respectively.

The third and final study that was used for comparison with the present data was that of Wang et al. (2005, [41]) and is shown in Figure 3.6. Wang et al. (2005, [41]) were able to improve upon the typical superposition method used previously by better accounting for no-slip boundary conditions at the surfaces of the drops. The previous

studies did not ensure these boundary conditions were satisfied at all points during the movement and interaction of the drops. It is interesting to note that the data produced by Wang et al. (2005, [41]) was significantly lower than the calculated results from the present work for a larger drop radius of 10 μm. The normal trend of larger collision efficiencies at larger drop sizes holds true for this case as well.

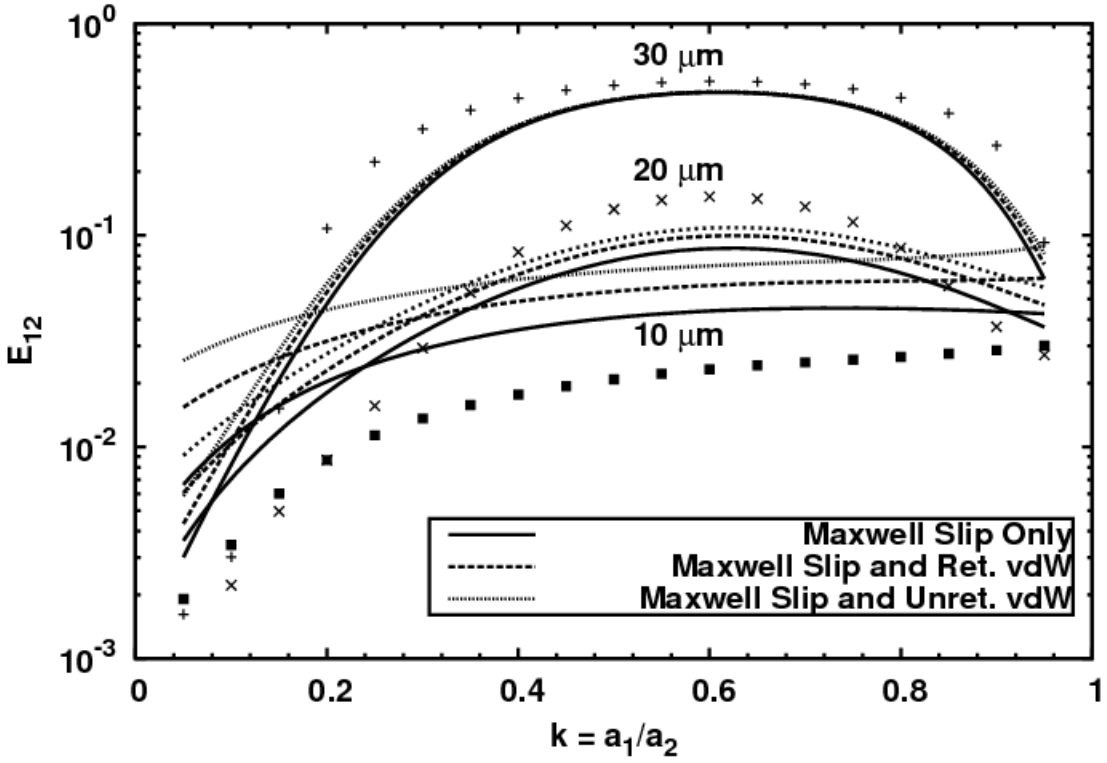

Figure 3.6 Comparison with data produced by Wang et al. (2005, [41]) for water drops in air. ■, x, and + represent their data for larger drop radii of 10 μm, 20 μm, and 30 μm, respectively.

Chapter 4

Conclusions

The research presented here has shown improvements made to both work dealing with slightly deformable drops and spherical drops, in the case of modeling raindrop growth. Through the inclusion of both gravitational and thermocapillary driving forces, it was possible to show that when small deformations of interacting drops are included in calculations for collision efficiency values, the deformations become important at different values of the drop-to-medium viscosity ratio and the drop-to-medium thermal conductivity ratio and at different values of N_V. By making allowances for small deformations of the drops, the collision efficiency values are lower when compared to the spherical drop results, possibly due to a pumping flow effect experienced by the drops as they are in close approach.

The second half of the work presented looked at collision efficiency calculations for spherical liquid drops, as applied to raindrop growth. Several earlier studies have looked at various aspects of calculating these collision efficiency values for solid spheres. The present work sought to carry out calculations that were as comprehensive as possible when it came to accounting for items in the overall force balance for the two interacting, liquid drops. This meant that the following were accounted for: Maxwell slip, van der Waals forces, lubrication forces, buoyancy, the weight of the drops, internal drop circulation, and hydrodynamic forces between the drops. Comparisons were then made with data generated by three previous studies. Over the range of drop sizes studied, the

previous studies seem to have overestimated the collision efficiency values by not including various components in the force balance that were included in the present work.

Future work should include detailed calculations performed for systems with practical applications. For example, the work completed for raindrop growth, when Maxwell slip and retarded van der Waals forces were included, could be incorporated into an existing atmospheric model to verify that the more comprehensive calculations better predict the formation of raindrops in air.

References

[1] Baldessari, F., Homsy, G.M., Leal, L.G., 2007. Linear stability of a draining film squeezed between two approaching droplets. J. Colloid Interf. Sci. 307, 188-202.

[2] Bazhlekov, I.B., Chesters, A.K., van de Vosse, F.N., 2000a. The effect of the dispersed to continuous-phase viscosity ratio on film drainage between interacting drops. Int. J. Multiphase Flow 26, 445-466.

[3] Bazhlekov, I.B., van de Vosse, F.N., Chesters, A.K., 2000b. Drainage and rupture of a Newtonian film between two power-law liquid drops interacting under a constant force. J. Non-Newtonian Fluid Mech. 93, 181-201.

[4] Berejnov, V., Lavrenteva, O.M., Nir, A., 2001. Interaction of two deformable viscous drops under external temperature gradient. J. Colloid Interf. Sci. 242, 202-213.

[5] Berejnov, V., Leshanksy, A.M., Lavrenteva, O.M., Nir, A., 2002. Spontaneous thermocapillary interaction of drops: effect of surface deformation at nonzero capillary number. Phys. Fluids 14, 1326-1339.

[6] Dai, Q., et al., 2016. Thermocapillary migration of liquid droplets induced by a unidirectional thermal gradient. Langmuir 32, 7485-7492.

[7] Davis, M.H., Sartor, J.D., 1967. Theoretical collision efficiencies for small cloud droplets in Stokes flow. Nature 215, 1371-1372.

[8] Davis, R.H., Schonberg, J.A., Rallison, J.M., 1989. The lubrication force between two viscous drops. Phys. Fluids A 1, 77-81.

[9] Fortelný, I., Jůza, J., 2014. Flow-induced coalescence in polydisperse systems. Macromol. Mater. Eng. 299, 1213-1219.

[10] Fortelný, I., Jůza, J., 2015. Consequences of the effect of matrix elasticity on the rotation of droplet pairs for collision efficiency. Colloid Polym. Sci. 293, 1713-1721.

[11] Hall, W.D., 1980. A detailed microphysical model within a two-dimensional dynamic framework: model description and preliminary results. J. Atmos. Sci. 37, 2486-2507.

[12] Hocking, L.M., 1959. The collision efficiency of small drops. Quart. J. R. Met. Soc. 85, 44-50.

[13] Hocking, L.M., Jonas, P.R., 1970. The collision efficiency of small drops. Quart. J. R. Met. Soc. 96, 722-729.

[14] Ismail, A.E., Loewenberg, M., 2004. Long-time evolution of a drop size distribution by coalescence in a linear flow. Phys. Rev. E 69, 046307 1-9.

[15] Janssen, P.J.A., Anderson, P.D., 2011. Modeling film drainage and coalescence of drops in a viscous fluid. Macromol Mater. Eng. 296, 238-248.

[16] Jonas, P.R., 1972. The collision efficiency of small drops. Quart. J. R. Met. Soc. 98, 681-683.

[17] Kang, Q., et al., 2006. Experimental investigations on interaction of two drops by thermocapillary-buoyancy migration. Int. J. Heat Mass Transfer 49, 2636-2641.

[18] Keh, H.J., Chen, L.S., 1992. Droplet interactions in axisymmetric thermocapillary motion. J. Colloid Interf. Sci. 151, 1-16.

[19] Klett, J.D., Davis, M.H., 1973. Theoretical collision efficiencies of cloud droplets at small Reynolds numbers. J. Atmos. Sci. 30, 107-117.

[20] Lin, C.L., Lee, S.C., 1975. Collision efficiency of water drops in the atmosphere. J. Atmos. Sci. 32, 1412-1418.

[21] Mahesri, S., Haj-Hariri, H., Borhan, A., 2014. Effect of interface deformability of thermocapillary motion of a drop in a tube. Heat Mass Transfer 50, 363-372.

[22] Nas, S., Tryggvason, G., 2003. Thermocapillary interaction of two bubbles or drops. Int. J. Multiphase Flow 29, 1117-1135.

[23] Pinsky, M., Khain, A., Krugliak, H., 2008. Collisions of cloud droplets in a turbulent flow. Part V: application of detailed tables of turbulent collision rate enhancement to simulation of droplet spectra evolution. J. Atmos. Sci. 65, 357-374.

[24] Pinsky, M., Khain, A., Shapiro, M., 2001. Collision efficiency of drops in a wide range of Reynolds numbers: effects of pressure on spectrum evolution. J. Atmos. Sci. 58, 742-764.

[25] Ramirez, J.A., Zinchenko, A., Loewenberg, M., Davis, R.H., 1999. The flotation rates of fine spherical particles under Brownian and convective motion. Chem. Eng. Sci. 54, 149-157.

[26] Rogers, J.R., Davis, R.H., 1990. The effects of van der Waals attractions on cloud droplet growth by coalescence. J. Atmos. Sci. 47, 1075-1080.

[27] Rother, M.A., 2007. Surfactant effects on thermocapillary interactions of deformable drops. J. Colloid Interf. Sci. 316, 699-711.

[28] Rother, M.A., 2009. Effects of incompressible surfactant on thermocapillary interactions of spherical drops. Int. J. Multiphase Flow 35, 417-426.

[29] Rother, M.A., 2013. The effect of surfactant redistribution on combined gravitational and thermocapillary interactions of deformable drops. Acta Astronautica 91, 55-68.

[30] Rother, M.A., Davis, R.H., 1999. The effect of slight deformation on thermocapillary-driven droplet coalescence and growth. J. Colloid Interf. Sci. 214, 297-318.

[31] Rother, M.A., Davis, R.H., 2001. The effect of slight deformation on droplet coalescence in linear flows. Phys. Fluids 13, 1178-1190.

[32] Rother, M.A., Davis, R.H., 2005. Breakup and capture of two sedimenting drops in a vertical temperature gradient. Phys. Fluids 17, 032103 1-12.

[33] Rother, M.A., Zinchenko, A.Z., Davis, R.H., 1997. Buoyancy-driven coalescence of slightly deformable drops. J. Fluid Mech. 346, 117-148.

[34] Rother, M.A., Zinchenko, A.Z., Davis, R.H., 2002. A three-dimensional boundary-integral algorithm for thermocapillary motion of deformable drops. J. Colloid Interf. Sci. 245, 356-364.

[35] Schlamp, R.J., Grover, S.N., Pruppacher, H.R., Hamielec, A.E., 1976. A numerical investigation of the effect of electric charges and vertical external electric fields on the collision efficiency of cloud drops. J. Atmos. Sci. 33, 1747-1755.

[36] Stark, J.K., Rother, M.A., 2016. Gravitational interactions of slightly deformable drops in a vertical temperature gradient. A presentation given at the Annual Meeting of the American Physical Society Division of Fluid Dynamics in Portland, OR.

[37] Stark, J.K., Rother, M.A., 2017. Gravitational collision efficiencies of small drops with application to raindrop growth. A presentation given at the Annual Meeting of the American Physical Society Division of Fluid Dynamics in Denver, CO.

[38] Vohl, O., Mitra, S.K., Wurzler, S., Diehl, K., Pruppacher, H.R., 2007. Collision efficiencies empirically determined from laboratory investigations of collisional growth of small raindrops in a laminar flow field. Atmospheric Res. 85, 120-125.

[39] Wang, H., Davis, R.H., 1993. Droplet growth due to Brownian, gravitational, or thermocapillary motion and coalescence in dilute dispersions. J. Colloid Interf. Sci. 159, 108-118.

[40] Wang, H., Davis, R.H., 1996. Collective effects of gravitational and Brownian coalescence on droplet growth. J. Colloid Interf. Sci. 178, 47-52.

[41] Wang, L., Ayala, O., Grabowski, W.W., 2005. Improved formulations of the superposition method. J. Atmos. Sci. 62, 1255-1266.

[42] Wozniak, G., 1991. On the thermocapillary motion of droplets under reduced gravity. J. Colloid Interf. Sci. 141, 245-254.

[43] Xie, H., et al., 2016. Simulation on thermocapillary-driven drop coalescence by hybrid lattice Boltzmann method. Microgravity Sci. Technol. 28, 67-77.

[44] Yiantsios, S.G., Davis, R.H., 1991. Close approach and deformation of two viscous drops due to gravity and van der Waals forces. J. Colloid Interf. Sci. 144, 412-433.

[45] Young, N.O., Goldstein, J.S., Block, M.J., 1959. The motion of bubbles in a vertical temperature gradient. J. Fluid Mech. 6, 350-356.

[46] Zhang, X., Davis, R.H., 1991. The rate of collisions due to Brownian or gravitational motion of small drops. J. Fluid Mech. 230, 479-504.

[47] Zhang, X., Davis, R.H., 1992. The collision rate of small drops undergoing thermocapillary migration. J. Colloid Interf. Sci. 152, 548-561.

[48] Zhang, S., Duan, L., Kang, Q., 2016. Experimental research on thermocapillary migration of drops by using digital holographic interferometry. Exp. Fluids 57, 113-125.

[49] Zhang, X., Wang, H., Davis, R.H., 1993. Collective effects of temperature gradients and gravity on droplet coalescence. Phys. Fluids A 5, 1602-1613.

[50] Zhou, H., Davis, R.H., 1996. Axisymmetric thermocapillary migration of two deformable viscous drops. J. Colloid Interf. Sci. 181, 60-72.

[51] Zinchenko, A.Z., Davis, R.H., 2005. A multipole-accelerated algorithm for close interaction of slightly deformable drops. J. Comput. Phys. 207, 695-735.

[52] Zinchenko, A.Z., Rother, M.A., Davis, R.H., 1997. A novel boundary-integral algorithm for viscous interaction of deformable drops. Phys. Fluids 9, 1493-1511.

Appendix

The governing equations for the inner region where two drops are nearly touching, namely the thin-film equations, are presented here in dimensionless form (Rother, Zinchenko, and Davis, 1997, [33]) with the modifications discussed in Chapter 2. These equations are presented for completeness.

Normal Stress Balance

$$p - \frac{\delta}{h^3} = 2 - \frac{1}{r}\frac{\partial}{\partial r}\left(r\frac{\partial h}{\partial r}\right) \tag{A.1}$$

Momentum Balance

$$f = -\frac{h}{2}\frac{\partial p}{\partial r} \tag{A.2}$$

Local Boundary Integral

$$f(r) = 4\int_0^\infty \phi(r', r)\left[\frac{u}{r'^2} - \frac{1}{r'}\frac{\partial u}{\partial r'} - \frac{\partial^2 u}{\partial r'^2}\right]dr' \tag{A.3}$$

Mass Continuity

$$\frac{\partial h}{\partial t} + \frac{1}{r}\frac{\partial}{\partial r}(rhu) = 0 \tag{A.4}$$

Integral Force Balance

$$\int_0^\infty \left(p - \frac{\delta}{h^3}\right) r dr = [\alpha_G \pm N_F \alpha_M]\cos\beta(t) \tag{A.5}$$

N_F was previously defined as

$$N_F = \pm \frac{(\hat{\mu}+1)\left(\hat{k}+2\right)(1+k)^2}{3kN_V}, \qquad (A.6)$$

where $N_V = \pm \frac{V_{G,12}^{(0)}}{V_{M,12}^{(0)}}$, $k = \frac{a_1}{a_2}$, $\hat{k} = \frac{k_d}{k_e}$, and $\hat{\mu} = \frac{\mu_d}{\mu_e}$.